Journal of Engineering and Applied Sciences 14 (24): 9788-9805, 2019
ISSN: 1816-949X

Experimental and Numerical Investigation of the Influence of Blade Geometries and Blade Number on the Performance of a Newly Developed Savonius-Style Wind Rotor

[1]Youssef Kassem, [2]Ali Sefik, [1]Hüseyin Çamur and [1]Abdulmajid A. Bahroun
[1]Department of Mechanical Engineering, Faculty of Engineering, Near East University, 99138 Nicosia, Cyprus
[2]Faculty of Engineering, Cyprus International University, 99138 Nicosia, Cyprus
yousseuf.kassem@neu.edu.tr, +90 (392) 2236464

Abstract: The objective of this study is to help design and model a new Savonius-style wind turbine that will have better performance than conventional Savonius wind turbines in terms of power. The geometrical parameters of the new Savonius-style were optimized to generate an optimum performance. An experimental investigation along with a numerical study using "Solid Works Flow Simulation" (SWFS) has been carried out to accomplish the objective. The static torque values of the rotor have been measured by experiments and calculated by numerical analysis and finally, they have been compared at different rotor positions ranging from 0°-360°. Experiments were conducted in front of a low-speed subsonic wind tunnel to determine the static and dynamic torques, the mechanical power as well as electrical power. In both studies, the new Savonius-style wind turbine was tested at various wind speeds ranging from 3-12 msec. Based on the experimental results, the newly developed Savonius-style resulted in a noticeable improvement in the power compared to that of the conventional Savonius rotors. Moreover, the results show that the long overlap significantly increases the power: by 40% compared with short overlap.

Key words: Conventional savonius rotor, flow characteristics, low wind speed, new Savonius-style, torque, power

INTRODUCTION

Energy demand of humanity has increased significantly in the last five decades and is likely to continue to do so in the foreseeable future. At the same time the world energy market faces risks and uncertainties in addition to the fact that the Earth's fossil fuel resources are not inexhaustible. This means volatilities in energy prices alongside concerns about energy supply security. Moreover, burning of fossil fuels to meet the energy demand is a major source of global warming and many other environmental problems. This unsustainable scenario makes it necessary either to develop new technologies or to improve the available ones, so as to better harness clean energy from renewable sources. It is in this sense that investigations in the area of wind power technology (Rolland *et al*., 2013b; Chong *et al*., 2013a, b; Obara *et al*., 2013; Saeidi *et al*., 2013; Danao *et al*., 2013; Morbiato *et al*., 2014).

Generally, horizontal axis wind turbines are used in energy production for grid-connected large utilities whereas vertical axis types are preferred for use in small scale domestic applications. Throughout the years, researchers have given a lot of attention to the horizontal axis wind turbine with outstanding achievements in terms of further developing the technology. On the other hand, current conventional designs for the vertical axis wind turbine do not satisfactorily meet the requirements of users in cases of off-grid power generation at low wind speeds. Therefore, investigation of small-scale turbines for distributed energy systems has become popular (Saeidi *et al*., 2013; Danao *et al*., 2013; Morbiato *et al*., 2014; Rolland *et al*., 2013a; Chong *et al*., 2013b; Balduzzi *et al*., 2012). The Savonius-style wind turbine has the potential to fulfil the needs users for such conditions. It has been reported that this type of wind turbine has lower efficiency when compared to its rivals. Nevertheless, Savonius-style wind turbines distinguish themselves from the other types targeting such markets because of its following advantages:

- Plain design which simplifies the manufacturing and maintenance processes and thus renders them to be more reliable devices

Corresponding Author: Youssef Kassem, Department of Civil Engineering, Faculty of Civil and Environmental Engineering, Near East University, 99138 Nicosia, Cyprus, yousseuf.kassem@neu.edu.tr, +90 (392) 2236464

- Low cut in and operating speeds which lead to lesser noise, wear and tear
- They can be installed on restricted-space locations such as rooftops, buildings or on top of communication towers
- There is no need for yaw mechanism since they operate independently from the wind direction (Roy and Saha, 2013a, b; Golecha *et al*., 2011; Abraham *et al*., 2012; Akwa *et al*., 2012a, b)

Now a days, in the rural areas of developing countries people tend to prefer a cost effective and low maintenance way of harnessing wind energy through the vertical axis wind turbines (Kamoji *et al*., 2009a, b; Gupta *et al*., 2008; Morshed *et al*., 2013; Gipe, 2004; Gupta and Biswas, 2011; Golecha *et al*., 2011; Roy and Ducoin, 2016; Goodarzi and Keimanesh, 2015). According to Kurt *et al*. (2014) and Uzun *et al*. (2014), the alternators or piezoelectric energy harvesters can be directly attached to the wind turbine blades to produce electricity. The Savonius vertical axis wind turbine is a novel fluid mechanical device that has been studied by numerous researchers Menet (2004), Kamoji *et al*. (2009a, b), Afungchui *et al*. (2010) and Sheldahl *et al*. (1978). These studies have mainly investigated the performance of small scale Savonius rotors by analysing the effect of various parameters such as aspect ratio, use of end plates, use of deflecting plates, overlap ratio and the number of blades (Saha *et al*., 2008; Mahmoud *et al*., 2012; Zhao *et al*., 2009; Nasef *et al*., 2013; Irabu and Roy, 2011; Morshed *et al*., 2013; Wenehenubun *et al*., 2015; Kacprzak *et al*., 2013; Roy and Saha, 2015; Sharma and Sharma, 2016; Mohamed *et al*., 2010; Tartuferi *et al*., 2015; Lee *et al*., 2016; Nasef *et al*., 2013; Roy and Saha, 2013, 2015; Kang *et al*., 2014; Akwa *et al*., 2012; Mohamed *et al*., 2010; Kianifar and Anbarsooz, 2011; Kianifar *et al*., 2010; Lin and Klimina, 2014; Emmanuel and Jun, 2011; Chen *et al*., 2012).

A new blade design for Savonius wind turbine has been investigated by numerical calculations and experiments. The goal of the present study is to investigate the effects of blade geometry, blade Number (N) and external overlap (e) on the power (performance) of new Savonius-style wind turbine. This research investigates the effect of wind speed on the static torque at different rotor positions ranging from 0°-360° in steps of 30° and is divided into two parts: in the numerical study of the new design of Savonius wind turbine, the fluid flow simulation Software SWFS is used to study the static torque characteristics at different wind speeds. Computational model is validated by the available experimental results in the literature and then a study of the static torque characteristics across the new design is conducted to obtain further information about the turbine's performance under low-velocity conditions. The performance of the new Savonius-style rotor is investigated by the numerical study of flow characteristics such as velocity, pressure, vorticity and turbulent dissipation rate. In the experimental study, an Electro Mechanical Dynamometer (EMD) is used to measure the static torque of the rotors. To ensure that the EMD measurements are reliable, the experimentally obtained mechanical power data of the conventional Savonius type wind turbine are compared to those of an identical wind turbine from the literature. In the second part, the effect of geometric and external overlap parameters on dynamic torque and power outputs (mechanical and electrical power) of the new Savonius-style wind turbineis examined experimentally by EMD at various wind speeds. In this research, an innovative Savonius-style wind rotor is designed to produce power for electricity demand in small buildings. This design is simple and cheap. The flowchart in Fig. 1 illustrates the analysis procedure of this study.

Numerical model: This study describes the computational domain and lateral boundary conditions, in addition to geometrical modelling and grid generation. Furthermore, a sensitivity analysis of the mesh is presented. Initially Savonius vertical axis wind rotor geometry by Saha *et al*. (2008) was modelled in solidworks and then solidworks flow simulation was utilised for the purpose of the study. Validation of the flow simulations were done by comparing to the experimental results reported by Saha *et al*. (2008). Then, the new Savonius-style rotors were designed and the static torque of the rotors and the flow characteristics were estimated numerically at various wind speeds and rotor positions.

Geometry and computational domain of the new Savonius-style rotor: Top view and isometric view of the new Savonius-style rotors are shown in Fig. 2. In the present investigation, two desks are placed on the top and bottom of the model. The distance between the two desks depends on the height of the rotor blades. Dimensions of design parameters are shown in Table 1.

In general, the physical domain includes the geometrical representation and boundary conditions which refer to the simplified form of the computational domain. The velocity inlet and outlet flow conditions are taken as the left and right boundaries, respectively. The top and bottom boundaries and the sidewalls are set as symmetrical conditions. The inlet velocity values are set

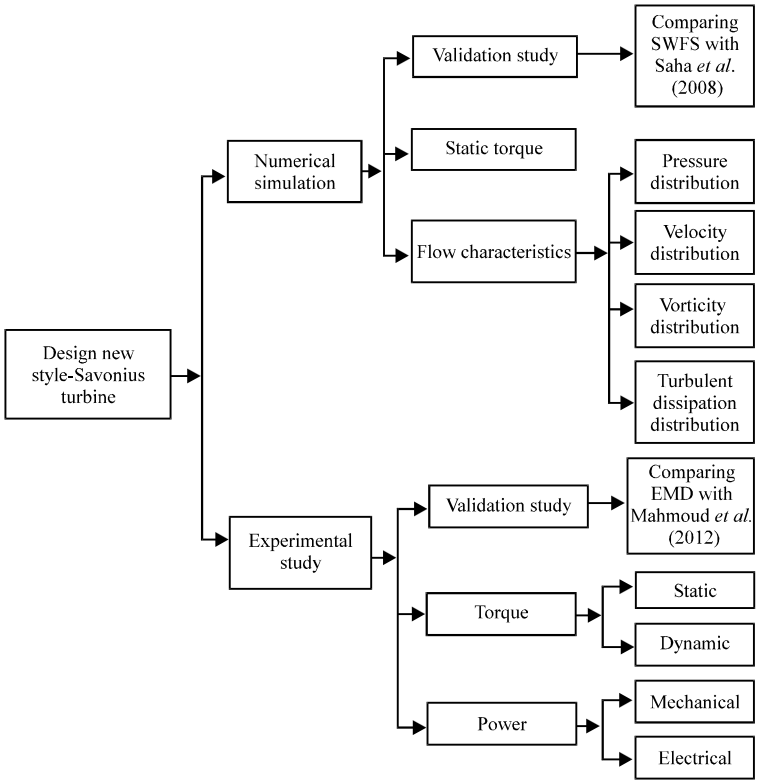

Fig. 1: Flowchart of analysis procedure of the present study

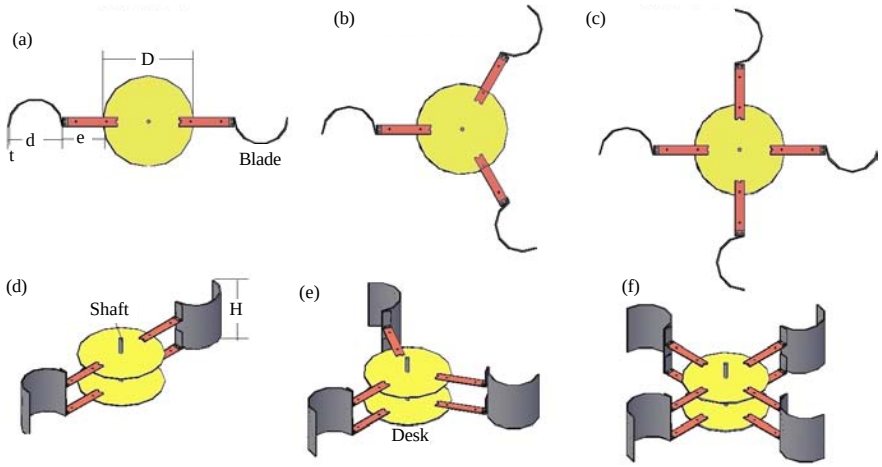

Fig. 2: The schematic shapes of the new Savonius-style rotors: a, d) 2-bladed rortor; b, e) 3-bladed rortor and c, f) 4-bladed rortor

for the velocity ranges of 3-12 msec. The outlet pressure is 101.325 kPa which means that the fluid exits the model to an environment of one atmospheric pressure. The walls of the computational domain are considered as wall boundary conditions. Figure 3 shows as example, the computational domain of the 4-bladed rotor with e = 150 mm. The wind enters the box (dimensions: 1500×1500×1200 mm), flows through the rotor blades and then exits through an outlet which is set to be environmental conditions. The rotor blade is placed in the middle of the box.

Mathematical formulation: The mathematical equations which govern physical phenomena can be composed of

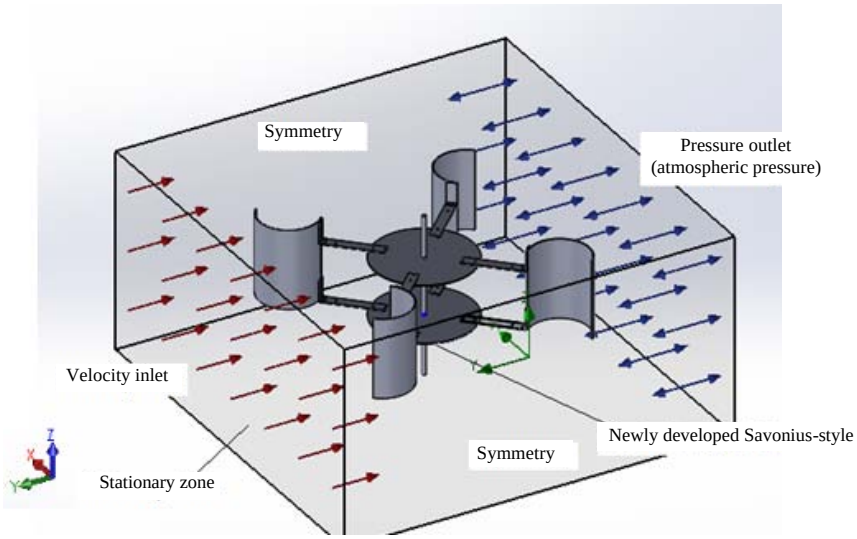

Fig. 3: Computational domains with boundary conditions

Table 1: Fixed and variable parameters of the design

Categories/design parameters	Values
Physical features	
Blade	Semi-cylindrical
No. of blades (N)	N = 2, 3 and 4 blades
Blade material	Light plastic (PVC)
Desk material	Fiberglass
Shaft material	Stainless steel
Dimensional	
Blade diameter (d)	d = 80, 100 and 160 mm
Blade thickness (t)	t = 3 mm
Desk Diameter (D)	D= 300 mm
Blade Height (H)	H = 300, 400 and 500 mm
External overlap (e)	e = 0, 50, 100 and 150 mm
Aspect ratio (β = H/d))	β = 1.875, 2.5, 3, 3.125, 3.75, 4, 5 and 6.25
Operational	
Rated wind speed (V)	V = 3, 4, 6, 8, 10 and 12 msec

dependent and independent variables and relative parameters in the form of differential Eq. 1-3. In this study, standard k-ε turbulence model has been used with logarithmic surface function in the analysis of turbulent flow. The Navier-Stokes equation governing the flow of air are obtained from the continuity equation, the equations of momentum, the transport equation of turbulent kinetic energy (k) and the transport equation of dissipation rate of turbulent kinetic energy (ε). SWFS solves Navier-Stokes equations with a finite volume discretization method. The governing equation can be written for incompressible unsteady flow in the Cartesian tensor notation as follows (Driss *et al*., 2010, 2011, 2014, 2015; Ammar *et al*., 2011). The continuity Eq. 1-3:

$$\frac{\partial \rho}{\partial t} + \frac{\partial (\rho u_i)}{\partial x_i} = 0 \tag{1}$$

The momentum Eq. 2:

$$\frac{\partial (\rho u_i)}{\partial t} + \frac{\partial (\rho u_i u_j)}{\partial x_j} = -\frac{\partial P}{\partial x_i} + \frac{\partial}{\partial x_j}\left[\mu\left(\frac{\partial u_j}{\partial x_j} + \frac{\partial u_j}{\partial x_i} - \frac{2}{3}\delta_{ij}\frac{\partial u_j}{\partial x_i}\right)\right] + \frac{\partial\left(-\rho\overline{u_i' u_j'}\right)}{\partial x_j} + F_i \tag{2}$$

Additional unknown term on the right hand side is called the Reynolds stresses $\left(-\rho\overline{u_i' u_j'}\right)$ and defined by:

$$-\rho\overline{u_i' u_j'} = \mu_t\left(\frac{\partial u_j}{\partial x_j} + \frac{\partial u_j}{\partial x_i}\right) - \frac{2}{3}\rho k\delta_{ij} \tag{3}$$

Furthermore, the Kronecker delta is defined by $\delta_{ij} = 0$ if $i \neq j$, else where $\delta_{ij} = 1$. In the present research, modified k-ε turbulence model with damping functions proposed by Lam and Bremhorst (1981). The transport equation of the turbulent kinetic energy k is written as follows:

$$\frac{\partial (\rho k)}{\partial t} + \frac{\partial (\rho k u_i)}{\partial x_i} = \frac{\partial}{\partial x_i}\left(\left(\mu + \frac{\mu_t}{\sigma_k}\right)\frac{\partial k}{\partial x_i}\right) + \tau_{ij}^R \frac{\partial u_i}{\partial x_j} - \rho\varepsilon + \mu_t P_B \tag{4}$$

And the transport equation of the dissipation rate of the turbulent kinetic energy ε is written as follows:

$$\frac{\partial (\rho\varepsilon)}{\partial t} + \frac{\partial (\rho\varepsilon u_i)}{\partial x_i} = \frac{\partial}{\partial x_i}\left(\left(\mu + \frac{\mu_t}{\sigma_\varepsilon}\right)\frac{\partial \varepsilon}{\partial x_i}\right) + C_{1\varepsilon}\frac{\varepsilon}{k}\left(f_1\tau_{ij}^R\frac{\partial u_i}{\partial x_j} + C_B\mu_t P_B\right) - f_2 C_{2\varepsilon}\frac{\rho\varepsilon^2}{k} \tag{5}$$

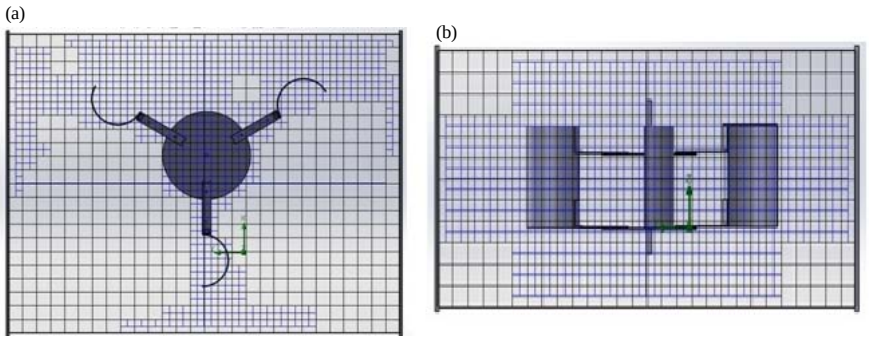

Fig. 4: Mesh for 3-bladed rotor

Table 2: Turbulence constants

Parameters	Values
C_μ	0.09
$C_{1\varepsilon}$	1.44
$C_{2\varepsilon}$	1.92
σ_k	1.0
σ_ε	1.3
σ_B	0.9
C_B	1 if P_B>1
C_B	0 if P_B<1

The laminar stress tensor is given by:

$$\tau_{ij} = \mu s_{ij} \tag{6}$$

and the Reynolds stress tensor is defined by:

$$\tau_{ij}^{R} = \mu s_{ij} - \frac{2}{3}\rho k \delta_{ij} \tag{7}$$

Where:

$$s_{ij} = \frac{\partial u_i}{\partial x_j} + \frac{\partial u_j}{\partial x_i} - \frac{2}{3}\delta_{ij}\frac{\partial u_k}{\partial x_k} \tag{8}$$

$$P_B = -\frac{g_i}{\sigma_B}\frac{1}{\rho}\frac{\partial \rho}{\partial x_i} \tag{9}$$

The turbulent viscosity is defined as follows:

$$\mu_t = \rho f_\mu C_\mu \frac{k^2}{\varepsilon} \tag{10}$$

In the standard k-ε turbulence model, the constants are C_μ, $C_{1\varepsilon}$, $C_{2\varepsilon}$, σ_k, σ_ε, σ_B and C_B. The numerical values of these constants are given in Table 2. Lam and Bremhorst's damping function f_μ, f_1 and f_2 are defined as:

$$f_\mu = \left(1 - e^{-0.025Ry}\right)^2\left(1 + \frac{20.5}{R_t}\right) \tag{11}$$

Where:

$$R_y = \frac{\rho\sqrt{k}y}{\mu} \tag{12}$$

$$R_t = \frac{\rho k^2}{\mu\varepsilon} \tag{13}$$

and y is the distance from point to the wall:

$$f_1 = 1 + \left(\frac{0.05}{f\mu}\right)^3 \text{ and } f_2 = 1 - e^{R_t^2} \tag{14}$$

Lam and Bremhorst's damping functions f_μ, f_1, f_2 decrease the turbulent viscosity and the turbulent kinetic energy but increase dissipation rate of the turbulent kinetic energy when the Reynold's number R_y based on the mean velocity of fluctuations and the distance from the wall becomes too small. When $f_\mu = 1$, $f_1 = 1$, $f_2 = 1$, the approach obtains the original k-ε model. This model has been used by Frikha *et al*. (2015) and led to satisfactory results.

Mesh study: A grid sensitivity analysis was carried out to reduce the computational time and guarantee a minimum discretization error from experimental results. This study describes the analysis for grids with various element sizes were and evaluation of the optimal grid size. The validity of the analysis was checked by comparing the results of numerical calculations with experimental results (Saha *et al*., 2008).

In this study, the local initial mesh option is used. This option allows specifying an initial mesh in a local region of the computational domain in order to resolve the model geometry better. The initial mesh is constructed by refining the basic mesh cells in accordance with the specified mesh settings. The basic mesh is formed by dividing the computational domain into slices by parallel planes which are orthogonal to the global coordinate system's axes. The computational mesh for the 3-bladed rotor model is shown in Fig. 4.

Table 3 illustrates the absolute error values obtained by comparing the calculated results with experimental ones for different wind speeds. The results indicate a small dependence on grid resolution and by considering

Table 3: Calculated errors from comparison of numerical and experimental results (Saha *et al*., 2008)

Wind speed (msec)/Cells No.	Torque (nm, numerical)	Torque (nm) (Saha *et al*., 2008)	Absolute error (%)
6			
18975	0.0142	0.0091	56.04
19560	0.0120		31.86
20117	0.0097		7.69
20943	0.0097		7.69
132795	0.0095		4.39
136683	0.0095		4.39
8			
132795	0.0376	0.0360	4.44

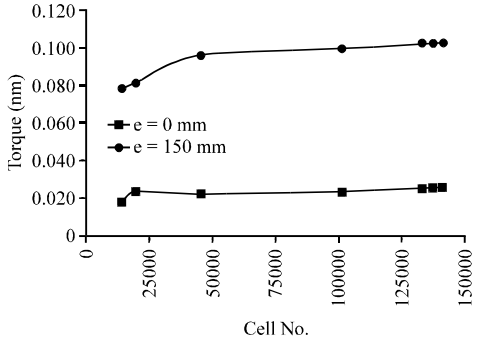

Fig. 5: Variation of static torque with respect to number of cells from the grid independence test at rotor angle of 0° (3-blade rotor, H = 500 mm, d = 160 mm)

run time of modelling; cell numbers around 132795 have a good agreement with experimental results by Saha *et al*. (2008).

The grid independence test was carried out by successively reducing the cell sizes in the grid. The stability of the results depends largely on the grid's resolution. In fact, the different numbers of mesh cells are used and the obtained results were compared with the experimental results, to find the optimal mesh density required.

Figure 5 shows the effect of refining the mesh size for the 3-bladed rotor for various external overlap ratios (e). Each level was solved in the simulation with the same set of input parameters. After a particular refining limit, the results do not show significant change. At this point, the grid independence in meshing is said to be achieved which for this particular case happens at 132,795 cells.

MATERIALS AND METHODS

Experimental study: This study present show the torque and power of the rotors were determined by using Electro Mechanical Dynamometer (EMD). In order to ensure and validate the experimental results, the mechanical power values measured by EMD are compared with the mechanical power results obtained by Mahmoud *et al*. (2012).The dimensions and the blade materials of the Savonius wind turbine utilised in the current study and the reference by Mahmoud *et al*. (2012) were identical. Furthermore, the wind speeds applied in these studies were of similar range.

The new Savonius-style rotor geometry: Three different configurations, namely 2-4 bladed rotors have been studied using semi-circular blades as shown in Fig. 1. The rotor blades are manufactured from light plastic (PVC) tubes with parameters given in Table 1. The shaft of the rotor is made of stainless steel with 20 mm diameter and it is 700 mm long. An attempt has been made to study a variety of rotor configurations with various aspect ratios (β) and external overlap lengths (e = 0, 50, 100 and 150 mm). Moreover, two desks were made from fibreglass with thickness of 5 mm and placed on the top and bottom of the model. The distance between the two desks depends on the height of blade rotor. The dimensions of the new Savonius-style rotors are shown in Table 1.

Test facility: To study the performance of the newly developed Savonius-style rotor, a low-speed open wind tunnel test facility has been constructed. The schematic diagram of this facility is shown in Fig. 6. The rotor axis is placed at a distance of 200 mm from the tunnel exit and it has a cross-section area of 700×700 mm. Air velocity at the exit of the tunnel was controlled by changing the input voltage with the help of a variac. All of the experiments were conducted with air velocity in the range of 0-15 msec. A four pitot tube was used to measure the air velocity with an accuracy of ±0.1 msec, while the rotational speed (RPM) of the rotor was measured with RPM sensor. Moreover, an Electro Mechanical Dynamometer (EMD) was used to measure the dynamic torque.

Experimental setup: The experimental set-up shown in Fig. 6 consists of the wind tunnel, wind turbine model and measurement devices, namely the pitot tube, RPM sensor and EMD. The Savonius rotor is placed at its proper position and is housed in a structure fabricated from mild steel plates. Two bearings (UC 204, NTN make) bolted to the mild steel plates supports the Savonius rotor. The seals are removed from the bearings and bearings are washed in petrol to remove any grease before mounting in order to reduce friction. The studs, nuts and bolts used in constructing the housing facilitate the replacement of various test geometries of the Savonius rotor and also help to determine the proper position of the rotor axis at the centre line of the wind tunnel. Furthermore, to increase the amount of voltage produced by the DC machine a

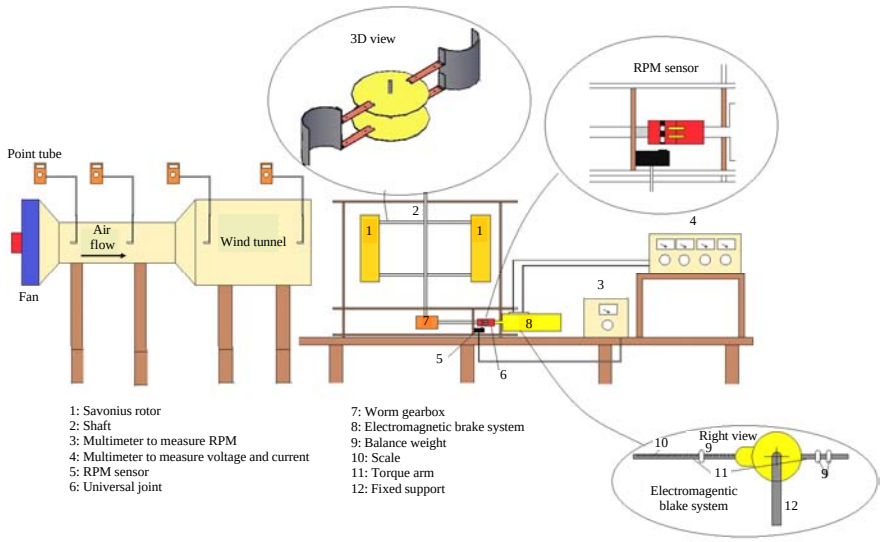

Fig. 6: Schematic diagram of the low-speed wind tunnel

gearbox was designed as shown in Fig. 6. The function of the gears is to increase the RPM input to the DC generator. Since, the dimensions of the rotor are known and the wind speed can be measured, the amount of torque the rotor delivers under different conditions can be evaluated.

The gear ratio of 1:10 was utilised in order to obtain optimum RPM needed for the particular generator. The rotors were attached to a gearbox which was attached to electromagnetic brakes system. An electromagnetic brakes system is used to measure force and torque from a rotating shaft and to measure the current and voltage produced by the rotor. The electromagnetic brakes system consists of water level, arms, weight and balance weight for measuring the output torque as shown in Fig. 6. Also, it consists of a Direct Current (DC) machine with the stator cradle-mounted on anti-friction bearings. The rotor is connected to the shaft of the machine under test. The stator is constrained from rotating by a radial arm of known length which is attached to a scale for measuring the force required to prevent rotation. The turbine is arranged with the stator mounted free to revolve but restrained from revolving by a brake arm attached to it and fastened to weighing scales. The RPM reader and multimeter are used to measure rotational speed of the DC shaft, voltage and current, respectively. The support eliminates all kinds of vibration and ensures stability of the setup during the experimental tests.

Experimental methods: The mechanical power is determined by measuring the mechanical torque on the rotating shaft and rotational speed at different wind speeds. The mechanical power can be estimated at each wind speed by:

$$P_m = T\omega \quad (15)$$

Where:

T = The mechanical Torque

ω = The angular speed

The angular speed is defined in rad/sec as:

$$\omega = \frac{2\pi n}{60} \quad (16)$$

where, n is the shaft rotational speed in rpm. The Force, F, shown on the scales of electromagnetic brakes system (Fig. 6) becomes mechanical Torque, T, when multiplied by the lever distance, d, from the centre of rotation. The mechanical torque is obtained in (nm) by:

$$T = Fd \quad (17)$$

Electrical Power, P_e generated by the wind turbine model is estimated by multiplying the measured current, I and Voltage, V. These parameters were recorded by multimeter device. The electrical power can be determined at each wind speed by:

$$P_e = IV \quad (18)$$

Validation study of experimental setup: A validation study was performed on the conventional Savonius rotor

Table 4: Comparison of validation study mechanical power of current study with mechanical power results by Mahmoud *et al.* (2012)

	Mechanical power results (W)								
	Mahmoud *et al.* (2012)			Current study			Absolute error (%)		
V (msec)	N = 2	N = 3	N = 4	N = 2	N = 3	N = 4	N = 2	N = 3	N = 4
6	0.23	0.26	0.19	0.25	0.28	0.20	8.69	7.69	5.26
8	0.52	0.50	0.48	0.45	0.55	0.52	9.62	10.00	8.30
10	2.70	2.20	1.70	2.95	2.00	1.55	9.25	9.10	8.82
12	3.40	3.85	2.50	3.80	4.30	2.80	11.76	11.68	12.00

by comparing the EMD results with the experimental results of Mahmoud *et al.* (2012), for three different rotors (2-4 bladed rotor) at four different velocities. A good way to perform a comparative study is to identify an output goal (mechanical power) for comparison and keep other parameters the same such as blade Height (H = 500 mm) and blade diameter (d = 100 mm). The geometries of the rotors were kept the same as well as the aspect ratio ($\beta = 5$) and the swept area. A single and double stage Savonius of Mahmoud *et al.* (2012) was placed in front of the suction type wind tunnel and the mechanical power of the rotors was measured. However, only a single-stage rotor has been studied in the present procedure. The results show a similar trend in both the validation study results and the experimental results of Mahmoud *et al.* (2012). Moreover, Table 4 summarises the mechanical power values of the present study for the mid-range of velocities, i.e., 6, 8, 10 and 12 msec. The absolute errors between the EMD results and the experimental results of Mahmoud *et al.* (2012) are within the acceptable limit of 5-12% which indicates the results are close to each other.

RESULTS AND DISCUSSION

The performance of the new Savonius-style rotor depends on various parameters such as the number of blades and blade geometry. The best way of optimizing these parameters is to carry out a number of tests on different types of rotors under low-speed conditions. Here, the numerical study and the experiments have been conducted with different types of rotors by varying the number of blades and blade geometry, so as to optimize the new Savonius-style rotor design. This study is organized as follows. Comparison of the static torque for numerical and experimental studies at various wind speeds and rotor positions is presented. The flow characteristics in terms of velocity, pressure, vorticity and turbulent dissipations. The experimental results showing the performance in terms of the dynamic torque and mechanical power at different number of blades and blade geometry are evaluated. Finally, the electrical power which the new Savonius-style wind rotor can produce, thus making it a good model for generating electricity in small commercial and domestic use.

Static torque of new Savonius-style rotors: Figure 7 shows the experimental and numerical static torque values for rotors with 2-4 blades at wind speeds of 4, 6 and 10 msec. It can be observed that the static torque increases with increases in the wind speed, external overlap and number of blades. The new Savonius-style rotor has positive static torque for all the rotor angles. The values obtained through numerical analysis have been found to be close to the experimental values, especially, for low wind velocities (4 and 6 msec).The deviation observed in the results at the highest wind velocity may have been caused by measurement errors and losses in the experimental study. Also, it is observed that for 2 and 3-bladed new Savonius-style rotors with external overlaps (e = 0 and 150 mm) there is a sharp increase in the static torque between rotor angles of 0°-90° and from 180°-270°. This sharp increase in the static torque coefficient is observed for rotors with all overlaps (e = 0, 50, 100 and 150 mm). This increase could be due to the distance between the rotor shaft and blades. For the 4-bladed rotor, it is observed that static torque decreases as the rotor angle changes from 0°-30° to reach its lowest value and then starts going up after 60° reaching its maximum value at 90°. Moreover, it is noticed that the static torque values remain nearly unchanged when the wind speed is at 4 msec as shown in Fig. 7. In general, Fig. 7 confirms the fact that Savonius rotors are self-starting, i.e., they start to rotate irrespectively of the wind flow direction as the torque value is positive for each rotor angle. Another important observation during the tests is that for the largest overlap (e>150 mm) the turbine shakes violently. This shows that at wind speeds higher than 4 msec, the turbine is unstable and this may reduce the performance of the turbine.

The experimental results (Fig. 7) clearly show that in the three models considered (2-4 bladed rotors) static torque values are rather low at low wind speeds but becomes considerably higher when the wind speed increases to 10 msec. This means that these wind turbine models have better rotational speed performance at high wind speeds. Moreover, according to the experimental results, the 3-bladed model is more stable than the 2 and 4 bladed ones. Also, the 3-bladed rotor with 160 mm blade diameter and 500 mm blade height achieves the highest static torque and is thus more efficient than the other geometries.

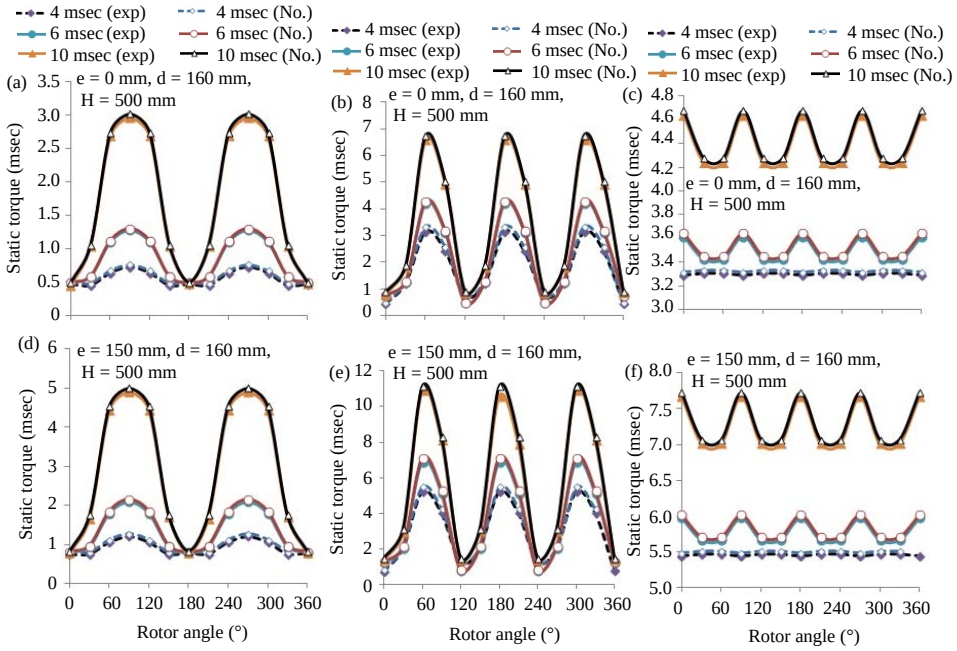

Fig. 7: Static torque vs. rotor positions: a, d) 2-blade; b, e) 3-blade and c, e) 4-blade

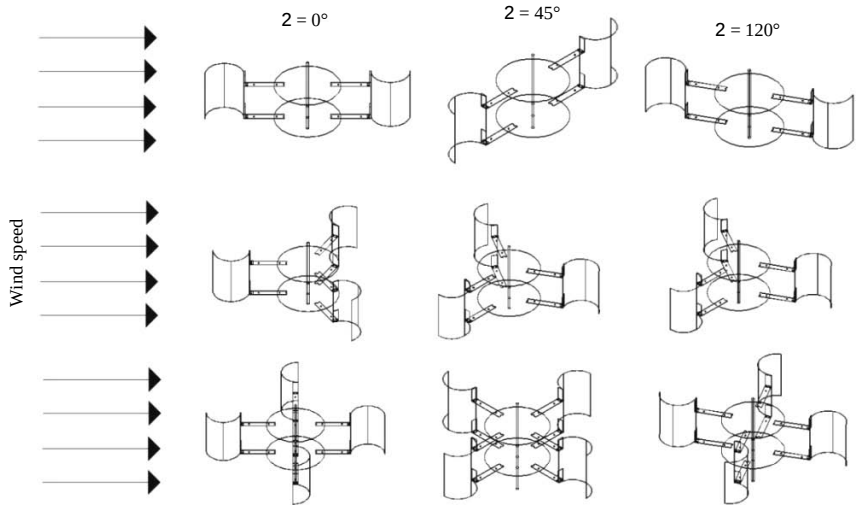

Fig. 8: Rotor positions

Flow characteristics of new Savonius-style rotors: In this study, the flow characteristics of the new Savonius-style wind rotor are discussed in terms of the velocity, pressure, vorticity values and the distribution of dissipation turbulent rate obtained through numerical analysis. In order to study the differences between the rotors, the flow characteristics have been analysed at the rotor for three different positions (0°, 45° and 120°) at various wind speeds (from 3-12 msec) as shown in Fig. 8.

Velocity fields for the 3-bladed rotor in the entire computational domain shown in Fig. 9 help to demonstrate some of the characteristic features of the unsteady flow. Once, the wind comes near the rotor the velocity magnitude starts to decrease. The higher velocity region occurs at the concave of the blade, especially at the blade which is on the pressure side. The back of the rotor side always creates a vacuum and remains at lowest velocity.

The deviation of drag forces caused by pressure differences on the blades of the Savonius wind turbine is

determined using the SWFS Software. Figure 10 shows pressure distributions for the new Savonius-style rotor with three blades. The pressure on concave blades is higher than the pressure on convex blades with result that the deviation of drag forces rotates the rotor.

Figure 11 shows the distribution of the turbulent dissipation rate on the plane defined by z = 0 mm. The wake characteristic of the maximum values of the turbulent dissipation rate values appear around the rotor axis and in the end plates of the buckets. Particularly for overlap length of 150 mm, these wakes appear on the convex surface of the buckets and cover the top of the superior bucket as presented in Fig. 11.

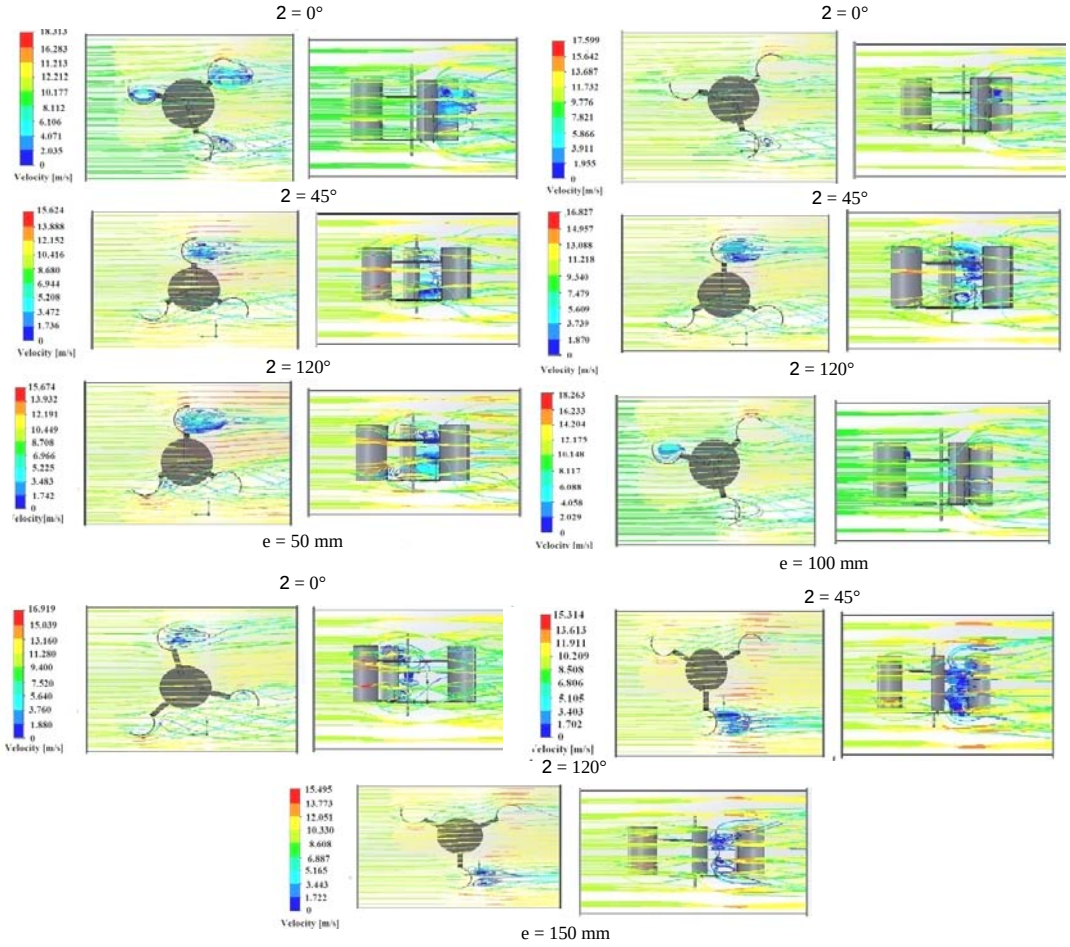

Fig. 9: Velocity distribution for the 3-bladed rotor versus rotor positions

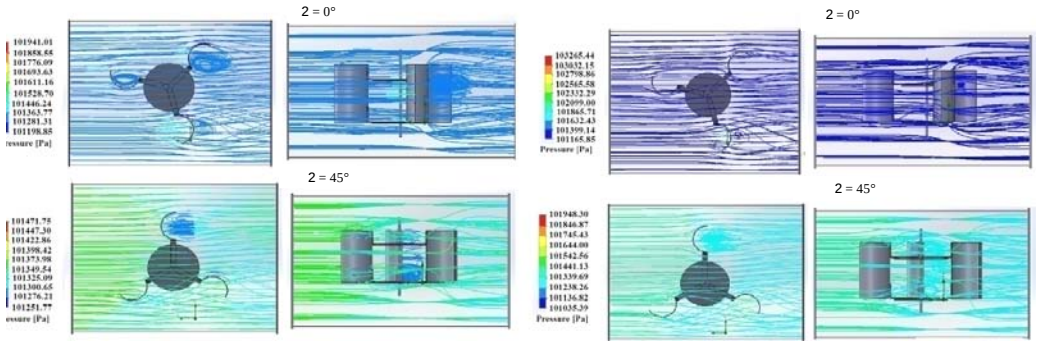

Fig. 10: Continue

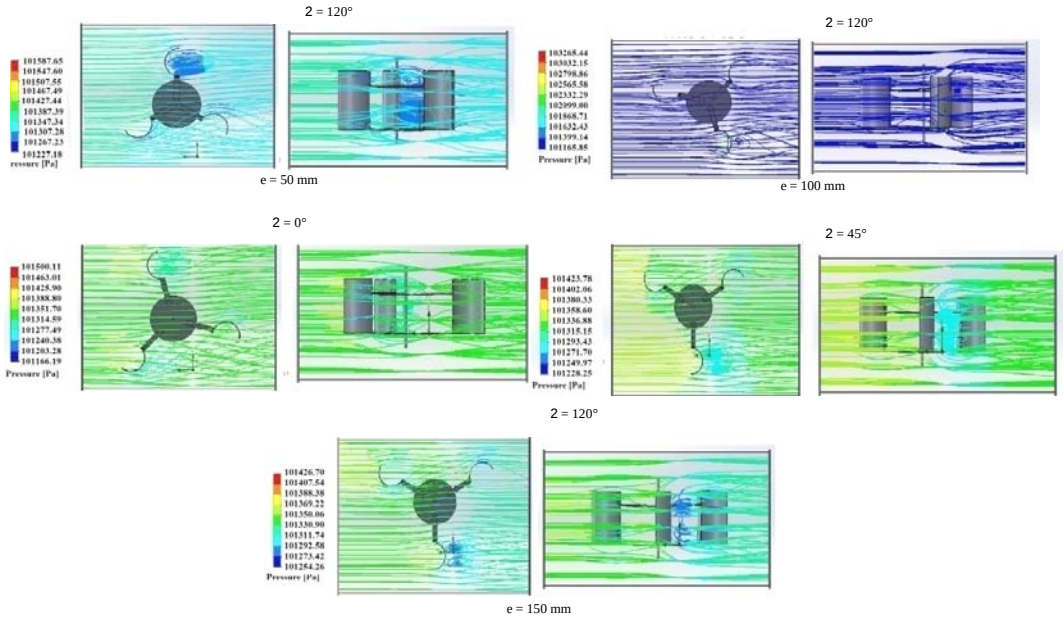

Fig. 10: Pressure distribution for 3-bladed rotor versus rotor positions

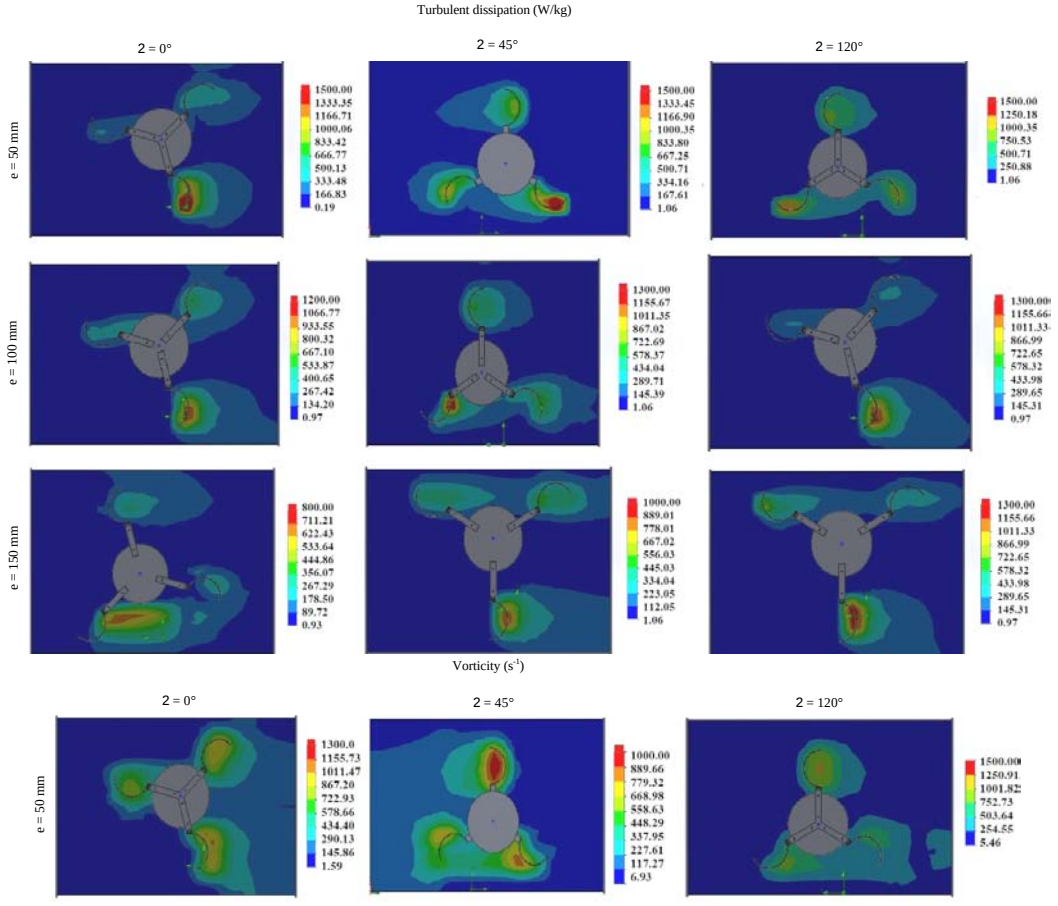

Fig. 11: Continue

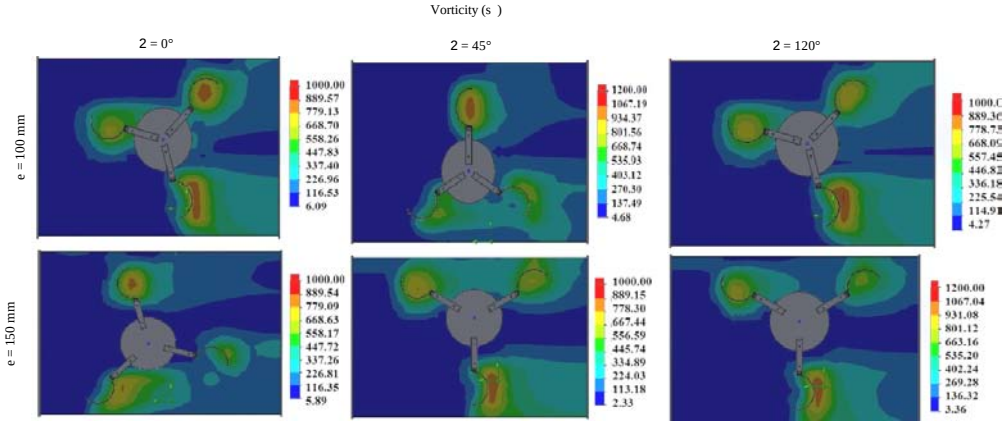

Fig. 11:Turbulent dissipation and vorticity for the 3-bladed rotor versus rotor positions

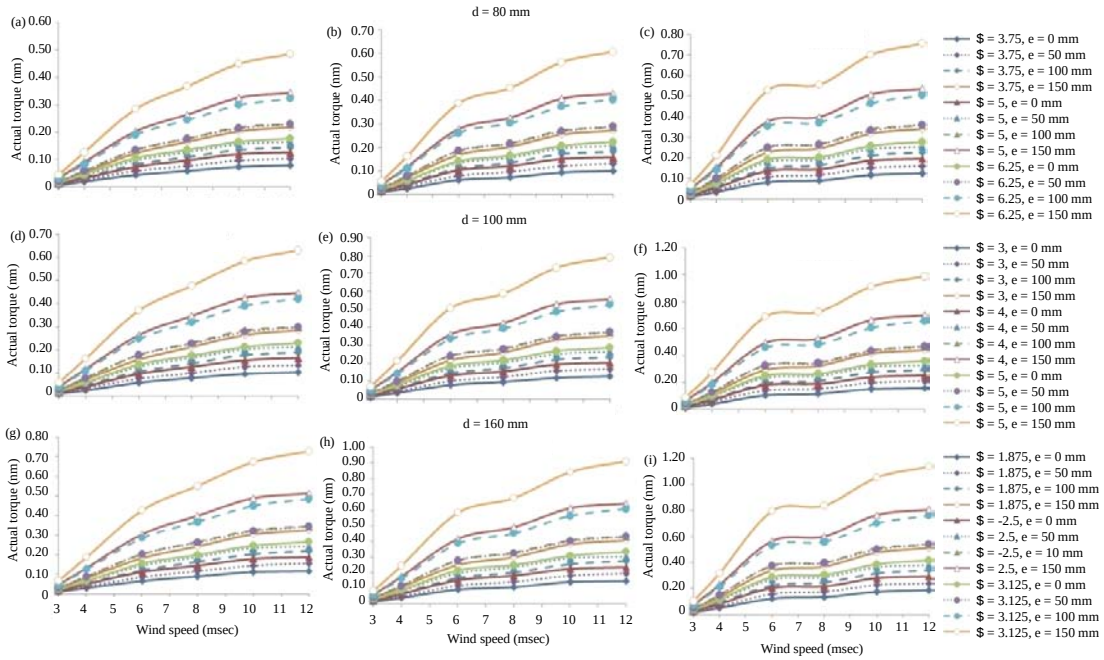

Fig. 12: Torque versus wind speed for different aspect ratios and blade numbers: a, d, g) 2-blade; b, e, h) 3-blade and c, f, i) 4-blade

Moreover, Fig. 11 shows the distribution of the vorticity on the plane defined by z = 0 mm. The wakes characteristics of the maximum values of the vorticity appear around the rotor axis and in the bucket sides. The comparison between these results confirms that the buckets design has a direct effect on the vorticity distribution. In fact, it's clear that the wakes characteristics of the maximum vorticity values become significant with the increase of the external overlap length.

Dynamic torque of new Savonius-style rotors: The experimental results describing the relationship between wind speeds and dynamic torque (actual torque) are as shown in Fig. 12. It is observed that the 4-bladed wind turbine model has a higher actual torque than that of the 2 or 3-bladed wind turbine. In addition, the actual torque increases as the wind speed, blade diameter aspect ratio and external overlap increases. From the results, it can be concluded that a four-bladed turbine should have about double or more weight to rotate when compared to a two and three blade turbine of the same size. In addition, the new Savonius-style with four blades has more drag force than the others at any position when the wind rotor is in rotational position. A wind turbine rotor with higher

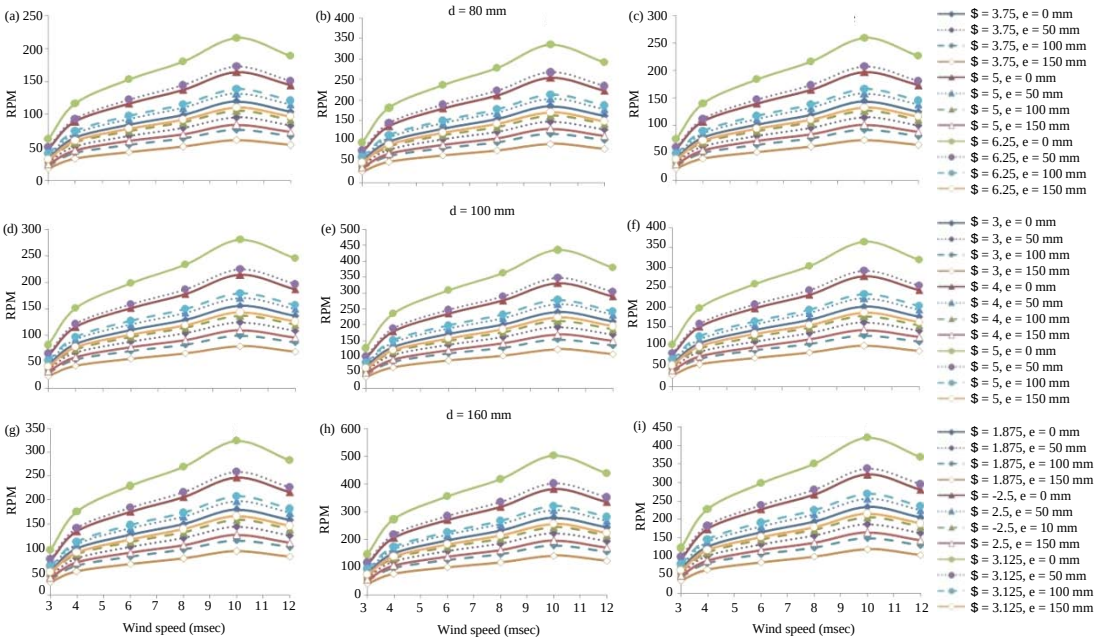

Fig. 13: RPM versus wind speed for different aspect ratios and blade numbers: a, d, g) 2-blade; b, e, h) 3-blade and c, f, i) 4-blade

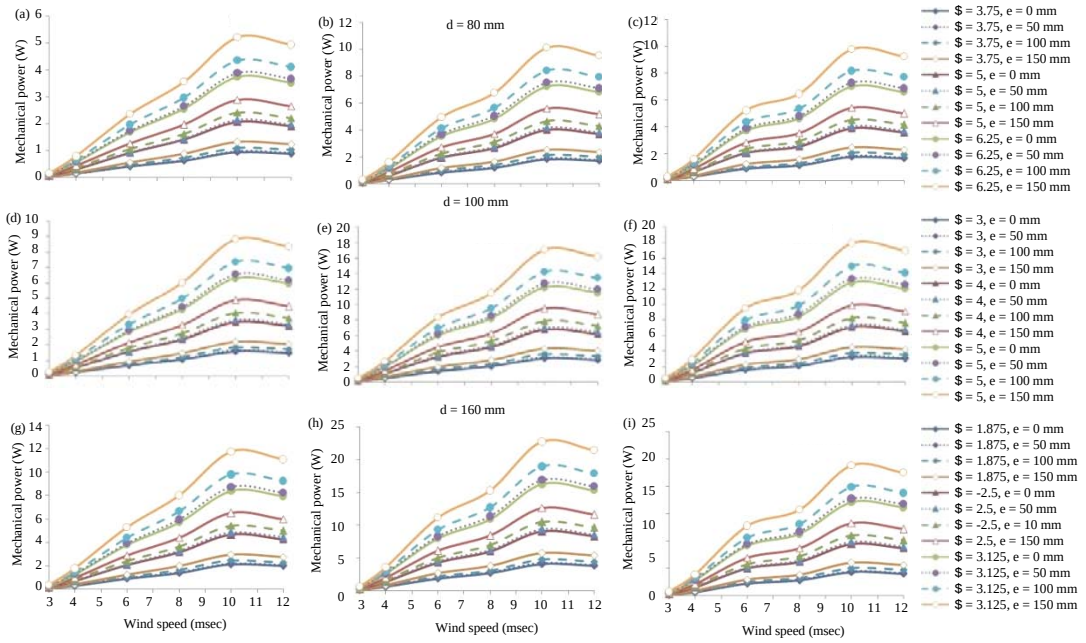

Fig. 14: Mechanical power versus wind speed for different aspect ratios and blade numbers: a, d, g) 2-blade; b, e, h) 3-blade and c, f, i) 4-blade

number of blades will deliver higher torque for the shaft of the turbine. Generally, the actual torque of the 4-bladed rotor is higher than the torque obtained in both the 3 and 4-bladed rotors. This may be because the net drag force acting on the rotor in the 4 blade case is higher than those for the 3 and 2-blade cases (Fig. 13 and 14).

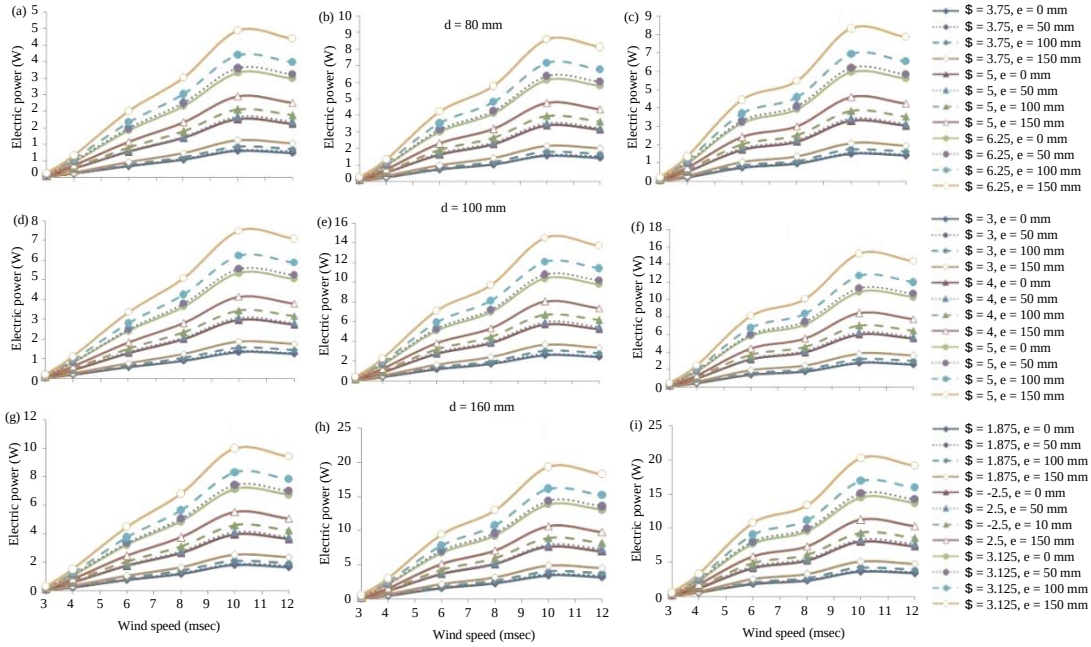

Fig. 15: Mechanical power versus wind speed for various aspect ratios, overlaps, blade numbers and blade diameters: a, d, g) 2-blade; b, e, h) 3-blade and c, f, i) 4-blade

Mechanical power of new Savonius-style rotors: Figure 13 shows the effects of the number of blades aspect ratio and external overlap length on the angular speed (RPM). As seen in Fig. 13, the 3-bladed wind turbine model has the highest RPM for all cases. In addition, it can be seen that all models have a fluctuating RPM ratio at low wind speeds and are more stable at wind speed of 10 msec. This shows that the wind turbine models reach an optimal rotational speed when the wind speed is around 10 msec. The variations of mechanical power related with wind speed are shown in Fig. 14. As Fig. 14 there show, for all of the three wind turbine rotor types, the mechanical power tends to vary polynomially with the wind speed. In the two-blade wind rotor, mechanical power will increase as wind speed increases, though it produces less power compared to the 3 and 4-blade rotors. In addition, it is observed that at wind speeds higher than 10 msec, the 3 and 4-blade wind turbine have lower rotation rates and less power for wind speeds in the range of 10-12 msec compared to the 3-blade turbine. That is to say, the 3-blade wind rotor has better performance than the 4 blade wind rotor. At 10 msec wind speed, power production from the 3-blade wind turbine increases steadily and the rotation produced can exceed the rotation of the 4-blade wind turbine. The 3-blade wind turbine model achieves better stability for similar power values than the 4-blade wind turbine.

Electrical power of new Savonius-style rotors: Figure 15 illustrates the variation in electrical power with wind speed for the investigated rotors. The power for the 3 and 4-bladed rotors is almost the same and it is higher than the power obtained from the 2-bladed rotor. This may be because the net drag force on the rotor in the 3 and 4 blade cases is higher than that in the 2-blade case. Moreover, when the number of blades is increased to four, the air which strikes on 1-blade get reflected back on the following blade, so that, the following blade rotates in the negative direction as compared to the preceding blade. Hence with an increase in the number of blades, the rotor performance decreases. It can be concluded from the experimental data that a 3-bladed system has better overall performance than the other two models. In addition as observed during testing, in the 4-blade turbine blade at wind speeds higher than 10 msec the blades started shaking. This shows that at high wind speeds, the turbine becomes unstable. Not only this may reduce the performance of the turbine, it may also even break down.

CONCLUSION

In the present study, the performance of a newly developed Savonius-style turbine was evaluated experimentally and computationally at low wind velocities of 3-12 msec. The results of this newly developed Savonius-style turbine are discussed and compared to

those of the conventional semi-circular 2 bladed Savonius turbine for the same blade geometries and wind speeds. The main observations are summarized as follows:

The torque of the newly developed Savonius-style turbine increases with increase in free stream wind velocity up to 12 msec. However, this increases the loading on the turbine blades which will reduce the performance of the turbine.

It is concluded that a 4-bladed turbine should have about double or more weight to complete full rotation compared to the 2 and 3-bladed turbines of the same size but a 4-bladed turbine achieves a pushing power that is nearly 4 times that of the 2-bladed turbine and double that of the 3-bladed turbine of the same size.

It is observed that the overlap length has a direct effect on the power of the rotors. Particularly, it has been noted that the power of the rotors increases with the increase of external overlap (e) length.

A comparative study of the simulated results versus experimental results was carried out and the static torque values at all rotor angles for all tested conditions are shown to be positive.

It is concluded that the optimum value of wind speed is 10 msec. In fact, it was observed during the tests that the turbine with the largest number of blades (4-blades) started shaking violently at higher wind speeds. This shows that at high wind speeds, turbines with four and larger numbers of blades are unstable. This may reduce the performance of the turbine and it may break down.

With the newly developed Savonius-style turbine a noticeable improvement in the maximum power is observed over the other models. The overall performance of the newly developed modified Savonius-style turbine is found to be superior to that of the conventional Savonius wind turbine.

SUGGESTIONS

The results suggest that compared to conventional Savonius rotors with or without an end plate, these rotors have better performance at low wind speeds and therefore can work well in Cyprus which generally has low winds. This suggests that this innovative idea is a suitable design to satisfy the main targets of the island.

ACKNOWLEDGEMENT

The researchers would like to thank the Faculty of Engineering, especially, the Mechanical Engineering Department of the Near East University for their support and encouragement.

NOMENCLATURE

C_B	:	Constant of the k-ε turbulence model (dimensionless)
$C_{1\varepsilon}$	:	Constant of the k-ε turbulence model (dimensionless)
$C_{2\varepsilon}$	:	Constant of the k-ε turbulence model (dimensionless)
C_μ	:	Constant of the k-ε turbulence model (dimensionless)
d	:	Blade diameter (mm)
D	:	Disk diameter (mm)
e	:	External overlap (mm)
F	:	Force acting on the rotor shaft (N)
F_i	:	Force per volume (nm^{-3})
f_1	:	Lam and Bremhorst damping function
f_2	:	Lam and Bremhorst damping function
f_μ	:	Lam and Bremhorst damping function
G_k	:	Production term of turbulence
g	:	Gravitational acceleration ($msec^2$)
H	:	Blade Height (mm)
I	:	Current (A)
k	:	Turbulent kinetic energy (J/kg^{-1})
l	:	Length (m)
m	:	Mass loaded on the pan (kg)
n	:	Shaft rotational speed (rpm)
N	:	No. of blades
P	:	Pressure (Pa)
P_B	:	Constant of the k-ε turbulence model (dimensionless)
P_e	:	Electrical Power (W)
P_m	:	Mechanical Power (W)
r_{shaft}	:	Radius of the shaft (m)
r_{rope}	:	Radius of the nylon string (m)
S	:	Spring balance reading (kg)
s_{ij}	:	Component of the strain rate tensor (s^{-1})
t	:	Blade thickness (mm)
T	:	Torque (nm)
u_i	:	Velocity components (msec)
u_i'	:	Fluctuating velocity components (msec)
u_j	:	Velocity components (msec)
u_j'	:	Fluctuating velocity components (msec)
u_k	:	Fluctuating velocity components (msec)
V	:	Velocity (m/sec)
V	:	Voltage (V)
X	:	Cartesian coordinate (m)
x_i	:	Cartesian coordinate (m)
x_j	:	Cartesian coordinate (m)
x_k	:	Cartesian coordinate (m)
Y	:	Cartesian coordinate (m)
Y	:	Distance from point to the wall (m)
Z	:	Cartesian coordinate (m)

ε : Dissipation rate of the turbulent kinetic energy (W/kg)
ω : Angular speed (rad/sec)
β : Aspect ratio (dimensionless)
μ : Dynamic viscosity (psec)
μ_t : Turbulent viscosity (psec)
ρ : Density (kg/m^3)
σ_ε : Constant of the k-ε turbulence model
σ_k : Constant of the k-ε turbulence model
σ_B : Constant of the k-ε turbulence model
δ_{ij} : Kronecker delta function (dimensionless)
τ_{ij} : Laminar stress tensor
τ_{ij}^R : Reynolds stress tensor

REFERENCES

Abraham, J.P., B.D. Plourde, G.S. Mowry, W.J. Minkowycz and E.M. Sparrow, 2012. Summary of Savonius wind turbine development and future applications for small-scale power generation. J. Renewable Sustainable Energy, Vol. 4, 10.1063/1.4747822

Afungchui, D., B. Kamoun, A. Helali and A.B. Djemaa, 2010. The unsteady pressure field and the aerodynamic performances of a Savonius rotor based on the discrete vortex method. Renewable Energy, 35: 307-313.

Akwa, J.V., G.A.D.S. Junior and A.P. Petry, 2012a. Discussion on the verification of the overlap ratio influence on performance coefficients of a Savonius wind rotor using computational fluid dynamics. Renewable Energy, 38: 141-149.

Akwa, J.V., H.A. Vielmo and A.P. Petry, 2012b. A review on the performance of Savonius wind turbines. Renewable Sustainable Energy Rev., 16: 3054-3064.

Ammar, M., W. Chtourou, Z. Driss and M.S. Abid, 2011. Numerical investigation of turbulent flow generated in baffled stirred vessels equipped with three different turbines in one and two-stage system. Energy, 36: 5081-5093.

Balduzzi, F., A. Bianchini, E.A. Carnevale, L. Ferrari and S. Magnani, 2012. Feasibility analysis of a Darrieus vertical-axis wind turbine installation in the rooftop of a building. Appl. Energy, 97: 921-929.

Chen, J, J. Kumbernuss, L. Zhang, L. Lu and H. Yang, 2012. Influence of phase-shift and overlap ratio on Savonius wind turbine's performance. J. Solar Energy Eng., Vol. 134, No. 1. 10.1115/1.4004980

Chong, W.T., A. Fazlizan, S.C. Poh, K.C. Pan, W.P. Hew and F.B. Hsiao, 2013b. The design, simulation and testing of an urban vertical axis wind turbine with the omni-direction-guide-vane. Appl. Energy, 112: 601-609.

Chong, W.T., S.C. Poh, A. Fazlizan, S.Y. Yip, C.K. Chang and W.P. Hew, 2013a. Early development of an energy recovery wind turbine generator for exhaust air system. Appl. Energy, 112: 568-575.

Danao, L.A., O. Eboibi and R. Howell, 2013. An experimental investigation into the influence of unsteady wind on the performance of a vertical axis wind turbine. Appl. Energy, 107: 403-411.

Driss, Z., A. Damak and M.S. Abid, 2015. Evaluation of the Savonius wind rotor performance for different external overlap ratios. Intl. J. Fluid Mech. Therm. Sci., 1: 14-21.

Driss, Z., G. Bouzgarrou, W. Chtourou, H. Kchaou and M.S. Abid, 2010. Computational studies of the pitched blade turbines design effect on the stirred tank flow characteristics. Eur. J. Mechanics-B/Fluids, 29: 236-245.

Driss, Z., O. Mlayeh, D. Driss, M. Maaloul and M.S. Abid, 2014. Numerical simulation and experimental validation of the turbulent flow around a small incurved Savonius wind rotor. Energy, 74: 506-517.

Driss, Z., O. Mlayeh, S. Driss, D. Driss, M. Maaloul and M.S. Abid, 2015. Study of the bucket design effect on the turbulent flow around unconventional Savonius wind rotors. Energy, 89: 708-729.

Driss, Z., S. Karray, H. Kchaou and M.S. Abid, 2011. CFD simulation of the laminar flow in stirred tanks generated by double helical ribbons and double helical screw ribbons impellers. Open Eng., 1: 413-422.

Emmanuel, B. and W. Jun, 2011. Numerical study of a six-bladed Savonius wind turbine. J. Sol. Energy Eng., 133: 1-5.

Frikha, S., Z. Driss and M.A. Hagui, 2015. Computational study of the diffuser angle effect in the design of a waste heat recovery system for oil field cabins. Energy, 84: 219-238.

Gipe, P., 2004. Wind Power: Renewable Energy for Home, Farm and Business. 2nd Edn., Chelsea Green Publishing, Vermont, USA., ISBN: 9781603581639.

Golecha, K., T.I. Eldho and S.V. Prabhu, 2011. Influence of the deflector plate on the performance of modified Savonius water turbine. J. Applied Energy, 88: 3207-3217.

Goodarzi, M. and R. Keimanesh, 2015. Numerical analysis on overall performance of Savonius turbines adjacent to a natural draft cooling tower. Energy Convers. Manage., 99: 41-49.

Gupta, R. and A. Biswas, 2011. CFD analysis of flow Physics and aerodynamic performance of a combined three-bucket Savonius and three-bladed Darrieus turbine. Intl. J. Green Energy, 8: 209-233.

Gupta, R., A. Biswas and K.K. Sharma, 2008. Comparative study of a three-bucket Savonius rotor with a combined three-bucket Savonius-three-bladed Darrieus rotor. Renewable Energy, 33: 1974-1981.

Irabu, K. and J.N. Roy, 2011. Study of direct force measurement and characteristics on blades of Savonius rotor at static state. Exp. Therm. Fluid Sci., 35: 653-659.

Kacprzak, K., G. Liskiewicz and K. Sobczak, 2013. Numerical investigation of conventional and modified Savonius wind turbines. Renewable Energy, 60: 578-585.

Kamoji, M.A., S.B. Kedare and S.V. Prabhu, 2009b. Experimental investigations on single stage modified Savonius rotor. Appl. Energy, 86: 1064-1073.

Kamoji, M.A., S.B. Kedare and S.V. Prabhu, 2009a. Performance tests on helical Savonius rotors. Renewable Energy, 34: 521-529.

Kang, C., H. Liu and X. Yang, 2014. Review of fluid dynamics aspects of Savonius-rotor-based vertical-axis wind rotors. Renewable Sustainable Energy Rev., 33: 499-508.

Kianifar, A. and M. Anbarsooz, 2011. Blade curve influences on the performance of Savonius rotors: Experimental and numerical. Proc. Inst. Mech. Eng. Part A. J. Power Energy, 225: 343-350.

Kianifar, A., M. Anbarsooz and M. Javadi, 2010. Blade curve influences on performance of savonius rotors: Experimental and numerical. Proceedings of the ASME 2010 3rd Joint US-European Fluids Engineering Summer Meeting Symposia-Parts A, B and C., August 1-5, 2010, American Society of Mechanical Engineers (ASME), Montreal, Quebec, Canada, ISBN:978-0-7918-4948-4, pp: 905-91.

Kurt, E., H. Gor and M. Demirtas, 2014. Theoretical and experimental analyses of a single phase Permanent Magnet Generator (PMG) with multiple cores having axial and radial directed fluxes. Energy Convers. Manage., 77: 163-172.

Lam, C.K.G. and K. Bremhorst, 1981. A modified form of the k-e model for predicting wall turbulence. J. Fluids Eng., 103: 456-460.

Lee, J.H., Y.T. Lee and H.C. Lim, 2016. Effect of twist angle on the performance of Savonius wind turbine. Renewable Energy, 89: 231-244.

Lin, C.H. and L.A. Klimina, 2014. CFD simulation and analysis for Savonius rotors with different blade configuration. AIP. Conf. Proc., 1637: 575-581.

Mahmoud, N.H., A.A. El-Haroun, E. Wahba and M.H. Nasef, 2012. An experimental study on improvement of Savonius rotor performance. Alexandria Eng. J., 51: 19-25.

Menet, J.L., 2004. A double-step Savonius rotor for local production of electricity: A design study. Renewable Energy, 29: 1843-1862.

Mohamed, M.H., G. Janiga, E. Pap and D. Thevenin, 2010. Optimization of Savonius turbines using an obstacle shielding the returning blade. Renewable Energy, 35: 2618-2626.

Mohamed, M.H., G. Janiga, E. Pap and D. Thevenin, 2011. Optimal blade shape of a modified Savonius turbine using an obstacle shielding the returning blade. Energy Convers. Manage., 52: 236-242.

Morbiato, T., C. Borri and R. Vitaliani, 2014. Wind energy harvesting from transport systems: A resource estimation assessment. Appl. Energy, 133: 152-168.

Morshed, K.N., M. Rahman, G. Molina and M. Ahmed, 2013. Wind tunnel testing and numerical simulation on aerodynamic performance of a three-bladed Savonius wind turbine. Intl. J. Energy Environ. Eng., 4: 1-14.

Nasef, M.H., W.A. El-Askary, A.A. Abdel-Hamid and H.E. Gad, 2013. Evaluation of Savonius rotor performance: Static and dynamic studies. J. Wind Eng. Ind. Aerodyn., 123: 1-11.

Obara, S., Y. Morizane and J. Morel, 2013. Study on method of electricity and heat storage planning based on energy demand and tidal flow velocity forecasts for a tidal microgrid. Appl. Energy, 111: 358-373.

Rolland, S., W. Newton, A.J. Williams, T.N. Croft, D.T. Gethin and M. Cross, 2013b. Simulations technique for the design of a vertical axis wind turbine device with experimental validation. Appl. Energy, 111: 1195-1203.

Rolland, S.A., M. Thatcher, W. Newton, A.J. Williams, T.N. Croft, D.T. Gethin and M. Cross, 2013a. Benchmark experiments for simulations of a vertical axis wind turbine. Appl. Energy, 111: 1183-1194.

Roy, S. and A. Ducoin, 2016. Unsteady analysis on the instantaneous forces and moment arms acting on a novel Savonius-style wind turbine. Energy Convers. Manage., 121: 281-296.

Roy, S. and U.K. Saha, 2013b. Review of experimental investigations into the design, performance and optimization of the Savonius rotor. Proc. Inst. Mech. Eng. Part A. J. Power Energy, 227: 528-542.

Roy, S. and U.K. Saha, 2013a. Review on the numerical investigations into the design and development of Savonius wind rotors. Renewable Sustainable Energy Rev., 24: 73-83.

Roy, S. and U.K. Saha, 2015. Wind tunnel experiments of a newly developed two-bladed Savonius-style wind turbine. Appl. Energy, 137: 117-125.

Saeidi, D., A. Sedaghat, P. Alamdari and A.A. Alemrajabi, 2013. Aerodynamic design and economical evaluation of site specific small vertical axis wind turbines. Appl. Energy, 101: 765-775.

Saha, U.K., S. Thotla and D. Maity, 2008. Optimum design configuration of Savonius rotor through wind tunnel experiments. J. Wind Eng. Ind. Aerodyn., 96: 1359-1375.

Sharma, S. and R.K. Sharma, 2016. Performance improvement of Savonius rotor using multiple quarter blades-A CFD investigation. Energy Convers. Manage., 127: 43-54.

Sheldahl, R.E., L.V. Feltz and B.F. Blackwell, 1978. Wind tunnel performance data for two-and three-bucket Savonius rotors. J. Energy, 2: 160-164.

Tartuferi, M., V. D'Alessandro, S. Montelpare and R. Ricci, 2015. Enhancement of Savonius wind rotor aerodynamic performance: A computational study of new blade shapes and curtain systems. Energy, 79: 371-384.

Uzun, Y., S. Demirbas and E. Kurt, 2014. Implementation of a new contactless piezoelectric wind energy harvester to a wireless weather station. Electron. Electr. Eng., 20: 35-39.

Wenehenubun, F., A. Saputra and H. Sutanto, 2015. An experimental study on the performance of Savonius wind turbines related with the number of blades. Energy Procedia, 68: 297-304.

Zhao, Z., Y. Zheng, X. Xu, W. Liu and G. Hu, 2009. Research on the improvement of the performance of Savonius rotor based on numerical study. Proceedings of the 2009 International Conference on Sustainable Power Generation and Supply, April 6-7, 2009, IEEE, Nanjing, China, ISBN:978-1-4244-4934-7, pp: 1-6.